Author Manuscript

Author Manuscript

Author Manuscript

Author Manuscript

HHS Public Access

Author manuscript

Nat Aging. Author manuscript; available in PMC 2023 April 14.

Published in final edited form as:

Nat Aging. 2022 August ; 2(8): 704–713. doi:10.1038/s43587-022-00268-y.

Age-associated suppression of exploratory activity during sickness is linked to meningeal lymphatic dysfunction and microglia activation

Dylan H. Goldman[1,2,3], **Taitea Dykstra**[1,2], **Igor Smirnov**[1,2], **Susan M. Blackburn**[1,2], **Sandro Da Mesquita**[4], **Jonathan Kipnis**[1,2,3], **Jasmin Herz**[1,2,✉]

[1]Center for Brain Immunology and Glia (BIG), Washington University in St. Louis, St. Louis, MO, USA.

[2]Department of Pathology & Immunology, Washington University in St. Louis, St. Louis, MO, USA.

[3]Neuroscience Graduate Program, University of Virginia, Charlottesville, VA, USA.

[4]Department of Neuroscience, Mayo Clinic, Jacksonville, FL, USA.

Abstract

Peripheral inflammation triggers a transient, well-defined set of behavioral changes known as sickness behavior[1–3], but the mechanisms by which inflammatory signals originating in the periphery alter activity in the brain remain obscure. Emerging evidence has established meningeal lymphatic vasculature as an important interface between the central nervous system (CNS) and the immune system, responsible for facilitating brain solute clearance and perfusion by cerebrospinal fluid (CSF)[4,5]. Here, we demonstrate that meningeal lymphatics both assist microglial activation and support the behavioral response to peripheral inflammation. Ablation of meningeal lymphatics results in a heightened behavioral response to IL-1β-induced inflammation and a dampened transcriptional and morphological microglial phenotype. Moreover, our findings support a role for microglia in tempering the severity of sickness behavior with specific relevance to aging-related meningeal lymphatic dysfunction. Transcriptional profiling of brain myeloid cells shed light on the

Reprints and permissions information is available at www.nature.com/reprints.

✉**Correspondence and requests for materials** should be addressed to Jasmin Herz. herz@wustl.edu.

Author contributions

D.H.G. primarily responsible for design and/or execution of experiments, analysis, and interpretation. T.D. performed analysis, interpretation of RNA-sequencing data, and design of figures. I.S. performed intra-cisterna magna injections and blinded experimenter. S.B. assisted with immunohistochemistry and ELISA and bred the mice. S.M. assisted with general experimental design, Visudyne ablation and AAV VEGF-C treatments. J.K. conceived project and advised overall work. J.H. assisted with experimental planning, design and execution; data discussion and interpretation; design of figures; and supervised revision and revised the manuscript. D.H.G, T.D. and J.H. wrote the manuscript.

Competing interests

J.K. is a member of a scientific advisory group for PureTech Heath. The other authors declare no competing interests.

Code availability

Computer code used for analysis are available from the authors upon reasonable request.

Reporting summary. Further information on research design is available in the Nature Research Reporting Summary linked to this article.

Extended data is available for this paper at https://doi.org/10.1038/s43587-022-00268-y.

Supplementary information The online version contains supplementary material available at https://doi.org/10.1038/s43587-022-00268-y.

Author Manuscript Author Manuscript Author Manuscript Author Manuscript

impact of meningeal lymphatic dysfunction on microglial activation. Furthermore, we demonstrate that experimental enhancement of meningeal lymphatic function in aged mice is sufficient to reduce the severity of exploratory abnormalities but not pleasurable consummatory behavior. Finally, we identify dysregulated genes and biological pathways, common to both experimental meningeal lymphatic ablation and aging, in microglia responding to peripheral inflammation that may result from age-related meningeal lymphatic dysfunction.

The well-documented behavioral shifts that occur in response to peripheral inflammation, known as sickness behavior, are largely conserved across vertebrate species, indicating high adaptive value. Yet, the lines of communication by which inflammatory signals in the periphery reach the brain, thereby influencing behavior, remain unclear[1–3]. Sickness behavior has been described as an altered motivational state characterized by decreased overall movement, lethargy and diminished interest in normal activities, such as eating and drinking. Interleukin-1β (IL-1β) has been studied in the context of sickness behavior for many decades. IL-1β alone is sufficient to induce a robust behavioral shift, and concurrence of elevated IL-1β protein expression within the CNS and sickness behavior is well documented[6–8]. Emerging evidence indicates, however, that the mechanisms underlying sickness behavior may contribute to major depressive disorders and bipolar disorders characterized by similar behavioral symptoms such as lethargy, apathy and reduced social interest[9–12]. Meta-analysis of studies using patient data reveals a significant correlation between elevated plasma IL-1β and major depressive disorder, a finding that has generated interest in anti-IL-1β therapeutic strategies for depression[12,13]. However, the impact of altering the balance of IL-1β/ IL-1Ra signaling in the CNS and increased systemic levels of IL-1β remains unclear[1,14–16].

The behavioral response to inflammation in animal models is known to be prolonged with age[17–19]. Although multiple etiological and neurobiological aspects may contribute to severity of sickness in patients during infections unrelated to the CNS, a predisposing risk factor for delirium, immobility, lethargy and cognitive decline is increased age[20–22]. Additionally, sedentary behavior is associated with increased incidence of new hospital-acquired disabilities in patients aged 60 years or older, indicating that severe sickness behavior may complicate functional recovery[23,24].

Lymphatic vessels in the meninges were recently shown to be important facilitators of CSF solute drainage, affect CSF–interstitial fluid exchange through the brain's glymphatic system and act as a key interface between the CNS and the peripheral immune system[4,25–27]. We have previously presented evidence that the deterioration of meningeal lymphatics with age contributes to the pathology of Alzheimer's disease in mouse models[5]. Largely unexplored, however, is the role of meningeal lymphatic vessels in facilitating neuroimmune communication in response to peripheral inflammation.

We hypothesized that modifications of meningeal lymphatic drainage would affect the ability of peripherally-derived inflammatory mediators to be delivered and/or cleared from the brain. We performed photodynamic ablation of meningeal lymphatics in adult mice by injecting the drug Visudyne into the CSF, followed by its photoactivation (ablation), to address the possibility that meningeal lymphatic vessels play a role in sickness behavior

Author Manuscript Author Manuscript Author Manuscript Author Manuscript

to peripheral inflammation. This procedure was previously shown to efficiently reduce meningeal lymphatic vessel coverage and drainage capacity[5,25] without affecting lymphatics outside the meninges[4]. Injections of Visudyne without the photoactivation step were used as a control (sham). To model sickness behavior induced by peripheral inflammation, we injected mice intraperitoneally (i.p.) with saline or IL-1β and assessed their drive to move and explore the open field arena over time (Fig. 1a). This approach enabled us to determine the impact of meningeal lymphatic vessel ablation on the severity and duration of sickness behavior. Ablation of meningeal lymphatics did not impact the total distance traveled by mice injected with saline (as a vehicle control) in the open field but led to a marked reduction in exploratory activity in mice that were injected with IL-1β (Fig. 1b,c). To determine if off-target effects of Visudyne activation contribute to this phenotype, we used either Visudyne with photoablation or photoactivation directed away from meningeal lymphatic vessels (Extended Data Fig. 1a,b). Notably, aiming at off-targeted regions in the meninges and comparing it to mice that received artificial CSF (aCSF) showed no phenotypic difference (Extended Data Fig. 1b), implicating that specifically targeting meningeal lymphatic vasculature resulted in decreased locomotor and exploratory activities and cannot be attributed to the generation of reactive oxygen species in the meninges themselves.

Additionally, we measured other sickness behaviors, including food and fluid intake and a preference for sucrose. Consumption of food after IL-1β-induced peripheral inflammation was not changed between sham and ablated groups (Fig. 1d,e). Although the absolute amount of fluid intake was significantly smaller in mice treated with IL-1β compared to their baseline (Fig. 1g), they did not show differences in consuming sucrose solution over water during sickness (Fig. 1h). Anhedonic behavior, defined by decreased sucrose preference, was also similar between sham and Visudyne-treated mice (Fig. 1h). Thus, lymphatic ablation affected the exploratory activity but not motivation for pleasurable stimulation such as sweet taste.

IL-1β is produced in the brain in response to peripheral inflammation, where, along with other inflammatory cytokines and paracrine signals, it is thought to influence behavioral shifts[6,8,18,28]. To determine whether local IL-1β signaling within the brain parenchyma and meninges contributes to sickness behavior, we used *Il1b* knockout (KO) mice. When injected i.p., IL-1β still sufficed to reduce exploratory activity in IL-1β KO mice (Fig. 1i,j). Although transcytosis of IL-1β across endothelial cells and direct action on brain parenchymal cells can occur[8,29], the blood–brain barrier is generally thought to limit this process[3,30]. These results suggested that peripheral IL-1β is sufficient to signal to brain and that IL-1β production within the CNS is not required to induce reduced activity in the open field.

To further establish the role of IL-1β signaling within the brain during sickness behavior, we bred mice with conditional KO of *Il1r1*, the gene that encodes the sole signaling receptor for IL-1β. To achieve conditional ablation of IL-1R1 from brain endothelial cells, we used adeno-associated virus (AAV)-BR1-Cre or AAV-BR1-GFP as a control vector to specifically target brain endothelium (Extended Data Fig. 2a). Depletion of *Il1r1* from several brain-resident cell types was achieved by crossing $Il1r1^{floxed}$ mice with neuron-specific ($Syn1^{Cre}$;

Author Manuscript Author Manuscript Author Manuscript Author Manuscript

Extended Data Fig. 2b), astrocyte-specific (*Gfap*^{CreER}; Extended Data Fig. 2c), or microglia- and macrophage-specific (*Cx3cr1*^{CreER}; Extended Data Fig. 2d) mice. We found that none of these conditional KO mice sufficed to alter sickness behavior in response to peripheral IL-1β. Yet, further experiments are needed to rule out incomplete Cre recombination and/or the cooperation of multiple cell types.

Although every brain cell population possesses the capability to secrete immunomodulatory signals including cytokines, recent work has indicated that microglia, as the brain's resident immune cells, play a key role in sickness behavior through the secretion of paracrine signals[1,31,32]. Because meningeal lymphatic vessel function is linked to paravascular CSF and interstitial fluid movement, it is possible that meningeal lymphatic vessels alter the availability of cytokines carried in the CSF to brain-resident microglia, thereby modifying their effects on the brain. To examine the impact of reduced meningeal lymphatic drainage on microglia activation, we injected saline or IL-1β into mice with intact (sham) or ablated meningeal lymphatics and harvested brains 2 h later for histological (Fig. 2a,b) and single-cell transcriptomic analysis (Fig. 2c–g). Microglial morphology is dynamic and responsive to immune activation; under homeostatic conditions microglia are ramified, whereas upon activation, their ramification becomes more simplified and ameboid[33]. Quantification of microglial complexity by Sholl analysis revealed that ablation of meningeal lymphatics is associated with a significantly more activated morphology at baseline and an impaired morphological shift of microglia to an activated form induced by IL-1β (Fig. 2a,b).

To assess microglia activation on a transcriptional level, CD11b^{+}-enriched cells were sequenced from brains of meningeal lymphatics-ablated and sham-treated mice (vehicle with photoactivation) following saline or IL-1β injection (Fig. 2c–g). Using single-cell RNA sequencing, we were able to distinguish between brain macrophages and microglia of different states (Extended Data Fig. 3a,b). We identified five microglial clusters, of which cluster 2 microglia showed a low expression of homeostatic genes and high number of upregulated genes associated with an activated state, such as *Ccl12*, *Ccl4* and *Socs3* (Extended Data Fig. 3c,d). Interestingly, cluster 2 microglia also presented higher levels of *Jun*, *Junb*, *Zfp36*, *Egr1* and *Btg2* (Extended Data Fig. 3c), which were recently described to occur artificially in brain myeloid populations when enzymatically digested[34]. However, in our data set, microglia from sham-and saline-treated groups contained only few cluster 2 microglia and were mostly induced by IL-1β treatment. Notably, cluster 2 was greatly expanded in IL-1β-treated groups compared to saline conditions, but this expansion slightly but significantly diminished with meningeal lymphatic photoablation (Fig. 2c,d). Genes previously implicated in sickness behavior, including *Il1b*, *Tnf* (tumor necrosis factor) and *Ptgs2 (*prostaglandin-endoperoxide synthase 2, commonly known as COX-2), but not *Il6*, were found elevated in microglia after induction of peripheral inflammation with IL-1β (clusters 0, 1, 2, 3 and 6 combined) (Fig. 2e). Furthermore, an increased expression of *Tnf* was observed upon meningeal lymphatic photoablation at baseline but was not further enhanced by IL-1β treatment relative to sham-treated controls. This is consistent with the histological analysis in Fig. 2a,b and suggests elevated microglia activation upon photoablation. In addition to their reduced transition to an activated state, we observed a diminished number of differentially expressed genes in response to IL-1β in mice with ablated meningeal lymphatics (Fig. 2f and Supplementary Table 1).

Author Manuscript Author Manuscript Author Manuscript Author Manuscript

To identify possible functional changes in microglia in response to peripheral inflammation associated with meningeal lymphatic ablation, we looked for biological processes enriched in differentially expressed genes unique to either the sham or the meningeal lymphatics-ablated response to IL-1β. The uniquely involved pathways of sham microglial genes were implicated in metabolic processes such as “ATP metabolic process”, “Mitochondrion organization”, “Mitochondrial respiratory chain complex assembly”, “Generation of precursor metabolites and energy” and “Oxidative phosphorylation”. Conversely, gene ontology terms for upregulated microglial genes after meningeal lymphatic ablation included “Cytokine secretion”, “Lymphocyte activation involved in immune response”, “T cell differentiation involved in immune responses”, “Cellular response to interferon-alpha” and “Myeloid leukocyte activation” (Fig. 2g). Overall, we observe a strong decrease in the number of unique enriched pathways (302 in sham and 42 in ablation), the number of genes identified per pathway and the relative statistical strength of enrichment between the sham and ablation groups responding to peripheral IL-1β (Supplementary Table 1). These findings suggest that an impairment of meningeal lymphatic drainage may lead to reduced microglia activation in response to peripheral IL-1β.

Because the response of myeloid cell depletion to peripheral IL-1β is unknown, we sought to address the impact of IL-1β on mouse behavior in the absence of microglia and macrophages by adding the colony-stimulating factor-1 receptor (CSF1R) antagonist PLX5622 into the feed for 2 weeks (Fig. 2h–j) and assessed exploratory activity upon i.p. injection with saline or IL-1β. Blockade of CSF1R efficiently depleted microglia as verified by immunohistochemistry (Fig. 2i) and has previously been shown to maintain the blood–brain barrier integrity[35]. It should be noted, however, that the treatment also reduces other myeloid cell populations[35–37]. Notably, we observed a heightened response to peripheral inflammation in microglia- and macrophage-depleted mice, suggesting a potential role for brain-resident myeloid cells in limiting the severity of exploratory behavior (Fig. 2j). These results are in line with recent findings showing decreased locomotor activity and voluntary wheel running after lipopolysaccharide injection in rats with altered microglia and macrophage responses[38]. It will be interesting to further understand whether meningeal lymphatic ablation (Fig. 1c) and myeloid cell depletion (Fig. 2j) can synergistically worsen sickness behavior. However, this will be challenging due to the ceiling effect observed in myeloid-depleted mice. Given the important role of monocytes and macrophages in modulating brain pathology and behavior, it will be worth investigating in future studies whether changes in these populations contribute to effects of sickness. Overall, and surprisingly, our data demonstrate that impaired meningeal lymphatic drainage reduces the microglial inflammatory response to peripheral IL-1β and that the lack of activated microglia (and other myeloid cells) aggravates the exploratory behavior induced by IL-1β.

Meningeal lymphatic function has been reported to decline with age[5]. To identify similarities between the effects of aging and of meningeal lymphatic ablation on the microglial response to peripheral inflammation, we sequenced $CD11b^+$ cells from the brains of aged mice 2 h after injection of IL-1β or saline and integrated the data sets with the previously described adult mouse single-cell RNA-sequencing data (Fig. 3a–e and Extended Data Fig. 3e,f). A comparison of the IL-1β response-associated differential gene expression in microglia across three conditions (adult (2.5-month-old) with intact meningeal

Author Manuscript Author Manuscript Author Manuscript Author Manuscript

lymphatics (sham), adult with meningeal lymphatic ablation (ablation) and 24-month-old (aged)) revealed fewer upregulated genes and more downregulated genes in the aged than in the sham condition, whereas the ablation group had the fewest in both directions (Fig. 3b and Supplementary Table 2). To identify aberrations in the microglial response to peripheral IL-1β-induced inflammation that were common to both the ablation and the aged conditions, we identified differentially expressed genes and enriched biological-process pathways in the ablation or aged responses compared to the sham response to IL-1β, on a cluster-by-cluster basis (Supplementary Table 3). The intersection of enriched biological pathways revealed modest overlap in homeostatic microglia (cluster 0) and robust overlap in IL-1β-responsive microglia (cluster 2) (Fig. 3c). A representative selection of microglial upregulated biological pathways common to the ablation and aged responses to peripheral IL-1β (Fig. 3d) was consistent with our assumption that although widespread activation is impaired by meningeal lymphatic ablation, there may be compensatory hyper-activation of a subset of microglia. Most of the gene ontology terms that were induced in microglia pointed to “Cell activation involved in immune response”, “Glia cell migration” and induction of proinflammatory cytokines (“Interleukin-1 beta production”, “Tumor necrosis factor production” and “Regulation of interleukin-6 production”). Unexpectedly, 25 gene pathways are shared between the ablation and aging IL-1β-responsive microglia in both lists of upregulated and downregulated pathways (Fig. 3e and Supplementary Table 3), indicating potential dysregulation resulting from the meningeal lymphatic impairment that is relevant in aging, and establishing avenues for further investigation into age-related pathologies and their link to meningeal lymphatic (dys)function[39].

Experimental treatment by means of AAV-mediated overexpression of VEGF-C can enhance the functioning of meningeal lymphatic vessels and improve glymphatic function in aged mice[5,40]. Following injection of AAVs into the CSF of 24-month-old mice, we allowed 1 month for expression of VEGF-C, which increased lymphatic vessel diameter in the meninges (Fig. 3f–i). Notably, we found that such treatment sufficed to increase exploratory activity in aged mice in response to peripheral IL-1β (Fig. 3i). Furthermore, aged mice treated with VEGF-C for meningeal enhancement of lymphatic function consumed the same amount of food compared to controls in response to IL-1β (Fig. 3j) and showed an unchanged preference for sucrose (Fig. 3k,l). These observations indicate that improving meningeal lymphatic vessel function with VEGF-C in aged mice leads to an ameliorated exploratory behavior that is not accompanied by improvement of hedonic deficits. Even though meningeal lymphatic vessel enhancement is the only major quantifiable effect of vascular endothelial growth factor C (VEGF-C) treatment in our studies, we cannot rule out direct effects on other VEGFR-3 expressing meningeal and brain blood endothelial cells. However, it is unlikely that microglia respond to VEGF-C because they lack the expression of *Flt4* and *Kdr* (Supplementary Tables 1–3).

Sickness behavior is a complex reaction that can result in multiple independent, neurological responses. In this investigation, we used an intraperitoneal injection of IL-1β in aged and young animals, which caused suppression of exploratory activity and food and fluid intake, but no other signs of sickness, such as anhedonia, were detected. Although the amount of IL-1β injected might not have been sufficiently high to provoke as severe of anhedonic disease in young male mice[41], it is also possible that the effects of IL-1β on “earned”

Author Manuscript Author Manuscript Author Manuscript Author Manuscript

sucrose reward could be attenuated but not “free” sucrose[42]. In older humans, excessive immobility associated with illness is strongly linked with worse medical outcomes; therefore, understanding this aspect of sickness behavior is a medical imperative[22,43]. Importantly, we discovered that lymphatic function enhancement improved exploratory activity in aged mice. These impairments mimic manifestations of older persons where mobility insufficiencies increase their need for care and support and adds to other difficulties such as maintaining a social or independent life[44]. A body of evidence suggests that older rodents are more susceptible to impaired interest in various pleasurable experiences, such as drinking sweet solutions and grooming[45,46], and are also increased in their susceptibility to sickness[17,47]. Although not statistically significant, a preliminary analysis suggests a trend linking increased meningeal lymphatic function in aged mice with less severe anhedonia which merits further study using different doses of IL-1β and additional methods to assess motivation of pleasurable stimuli[48].

These findings emphasize the broad contribution of meningeal lymphatic vessels in facilitating healthy neurological function, including the behavioral response to peripheral immunological stimuli. We speculate that this impact on behavior is due to reduced glymphatic function, impairing the perfusion of soluble signals. Ablation of meningeal lymphatics, however, may also impact the diverse immune cell populations present in the meninges, which could contribute to behavioral output[5,26]. Because proinflammatory cytokines are capable of inducing sickness behavior, and because microglia can be a source of proinflammatory cytokines in response to peripheral inflammation, previous studies have proposed that the release of proinflammatory factors secreted by microglia is the driving force responsible for altering behavior through yet-unknown downstream mechanisms that alter neuronal activity[31].

In summary, we demonstrate that the acute behavioral depression of exploratory activity in response to peripheral IL-1β does not depend upon de novo production of IL-1β in the brain. Further, we show that disruption of meningeal lymphatics in mice exacerbates their behavioral response to peripheral inflammation induced by IL-1β while also impairing microglial activation, as assessed by their morphology and transcriptional state. We present new lines of evidence suggesting that microglial activation upon peripheral inflammation is necessary for tempering the behavioral response rather than for initiating or sustaining it. In addition, we demonstrate that experimental enhancement of meningeal lymphatic function suffices to improve movement in sick, aged mice. Lastly, we identify pathways and genes with similar microglial dysregulation in both adult mice with ablated meningeal lymphatics and aged mice in response to peripheral IL-1β. Our new findings show that both microglial depletion and impairment of microglial activation worsens behavioral alterations induced by IL-1β. Further studies should stratify in improving lymphatic dysfunction at the brain border to modulate cytokine exchange for the fine tuning of neuronal activity in mood disorders, sickness behavior and inflammaging, but also reevaluate the role of microglial activation.

Author Manuscript Author Manuscript Author Manuscript Author Manuscript

Methods

Mice.

All mice used were on a C57BL/6 background and bred in-house using mice purchased from The Jackson Laboratory (Jax). Experiments were performed with male mice between 2 and 4 months or 24 months of age. Mice were maintained under specific pathogen-free conditions, with an ambient temperature of 21 °C and ~50% humidity, on 12 h light/dark cycles and ad libitum access to food and water. For conditional KO experiments *Il1R1*$^{flox/flox}$ (B6.129(Cg)-*Il1r1*$^{tm1.1Rbl}$/J, Jax stock number 028398) mice were crossed with *Syn1*^{Cre} (B6.Cg-Tg(Syn1-cre)671Jxm/J, Jax stock number 003966), *Cx3cr1*^{CreER} (B6.129P2(C)-*Cx3cr1*$^{tm2.1(cre/ERT2)Jung}$/J, Jax stock number 020940) or *GFAP*^{CreER} (B6.Cg-Tg(GFAP-cre/ERT2)505Fmv/J, Jax stock number 012849) strains to heterozygosity, or administered AAV as described in AAV delivery to induce conditional deletion of *Il1r1* on brain endothelium. Cre-negative littermates were used as control mice for respective experiments. C57BL/6 J (Jax stock number 000664), IL-1β KO mice were ordered from Jax (C57BL/6J-*Il1b*^{em2Lutzy}/Mmjax, Jax stock number 032998) and allowed 2 weeks habituation before use in experiments. Aged mice were provided by the National Institutes of Health/National Institute on Aging. All experiments were approved by the Institutional Animal Care and Use Committees of the University of Virginia (protocol 3922) and Washington University in St. Louis (protocol 20-0043).

Tamoxifen treatment.

Tamoxifen-inducible Cre mouse lines, including Cre-negative littermates, were provided tamoxifen chow (ENVIGO, TD.130856, 250, 2016, red) for 2 weeks to induce conditional excision of floxed alleles. Tamoxifen chow was then replaced with normal chow for 2 weeks before testing to reduce off-target effects of tamoxifen treatment.

IL-1β-induced sickness behavior.

Recombinant murine IL-1β was obtained from PeproTech (211-11B) and resuspended in sterile saline. Mice were administered 1 μg IL-1β or saline vehicle in 100 μl i.p. injection for all sequencing and adult mouse behavior. Due to higher susceptibility of IL-1β in aged mice, the dose was reduced to 0.5 μg.

Immunohistochemistry, imaging and quantification.

Mice were killed by an overdose of pentobarbital sodium solution (e.g., Euthasol, Virbac, 200-071) and then transcardially perfused with 10 ml of ice-cold PBS (Gibco, 14190-136) with 10 U ml^{-1} heparin (Sagent, 400-30). Mouse brain and skull cap were drop fixed in 4% paraformaldehyde (Thermo Fisher Scientific, 19202) in PBS at 4 °C for 24 h. Following fixation, dura was dissected from skull cap and stored in PBS containing sodium azide (0.02%) (Thermo Fisher Scientific, 71448-16) until further processing. Brain tissue was dehydrated in 30% sucrose solution then frozen in optimum cutting temperature compound (Thermo Fisher Scientific, 23-730-571), and 60-μM sections were cut on a cryostat (Leica, 3050 S). Floating sections were stored in PBS containing sodium azide (0.02%) until further processing. Tissue samples were permeabilized in PBS containing

Author Manuscript Author Manuscript Author Manuscript Author Manuscript

0.2% Tween-20 (Thermo Fisher Scientific, BP337-500) and 0.1% Triton X-100 (Thermo Fisher Scientific, BP151-500) and blocked with 2% chicken serum (Sigma-Aldrich, C5405) in PBS containing 0.1% Tween-20 and 0.05% Triton X-100 for 1 h. Samples were incubated overnight at 4 °C with primary antibodies in PBS containing 2% chicken serum, 0.1% Tween and 0.05% Triton X-100. Primary antibodies include: goat polyclonal anti-Iba1 (1:200, Abcam, ab5076) and rat anti-Lyve1-eFluor660 (1:200, eBioscience, 50-0443, clone ALY7). Following primary antibody incubation, tissue was washed three times in PBS containing 0.1% Tween and 0.05% Triton X-100 then incubated in fluorescently-conjugated chicken anti-Goat IgG Alexa Fluor 647 (1:1,000, Invitrogen, A21469) for 2 h at room temperature. Tissue was then washed three times and incubated in DAPI for 10 min. Tissue was then mounted on microscope slides using Aqua-Mount (Thermo Fisher Scientific, TA125) or Prolong Gold (Thermo Fisher Scientific, P36931). Brain tissue was imaged using an Olympus FV1200 Laser Scanning Confocal Microscope and FV10-ASM program. Meninges were imaged using an Olympus VS200 digital slide scanner using VS200 AS. Image quantification was performed using the FIJI package for ImageJ. Sholl analysis was performed by manually isolating individual microglia and using the Sholl analysis plugin for ImageJ. Meningeal lymphatic vessel diameter was quantified by manually annotating on at least 100 points along the superior sagittal sinus-adjacent lymphatic vessels. All analysis was performed blinded to conditions and the experimenter was unblinded following statistical analysis.

Behavioral testing and analysis.

Mice were habituated to the testing room in their home cages for at least 1 h before behavioral testing. All behavior data collection and analysis was performed by an experimenter blinded to the identity of experimental groups. Data tables were created in Excel (Microsoft) and imported into Prism (GraphPad).

Open field test.—Repeated exploratory assessment was carried out during daylight hours. Mice were placed individually in the corner of a 35 × 35-cm arena, recorded for 10 min, and then returned to their home cage. Mice were tested four times at 1, 2, 3 and 6 h after IL-1β or saline treatments. Following each open field test, mice were returned to their home cage and remained in the testing room until all time points had been collected. The open field boxes were cleaned with 70% ethanol after each test. Behavioral testing was recorded on video and mouse tracking and analysis performed using EthoVision XT (Noldus) software to quantify exploratory activity.

Sucrose preference.—During adaptation (starting at 5 pm), mice were given two regular bottles, one containing 1% sucrose (w/v) (VWR, SS1020) and one with regular drinking water in their home cage for 48 h (the positions of the bottles were switched after 24 h). Mice were then transferred individually into a SPT apparatus consisting of 5 chambers of the same size (10 × 24 × 13 cm; W × L × H) with two liquid feeding tubes containing 1% sucrose or regular water to adapt to the chambers for 24 h (5 pm to 5 pm)[49]. As circadian rhythm influences drinking behavior, the following procedures were performed at night (9 pm to 9 am) and mice were returned to their home cage in the intervals between baseline and preference measurements. After performing two baseline assessments for 12 h, mice

Author Manuscript Author Manuscript Author Manuscript Author Manuscript

were injected with IL1-β and their preference tested. The consumption of sucrose intake relative to the total intake of sucrose and water was measured to determine the preference for sucrose on each day. The second baseline with switched bottle locations was required to ensure mice were properly habituated. All mice had ad libitum access to standard chow during the behavioral experiment.

Food consumption.—Mice were single-housed and food deprived for 14 h (7 pm to 9 am) before IL-1β injections. Standard chow pellets were weighed and placed on the food hopper and 2 pieces (~10 g) on the ground. After 3 and 6 h, food was measured and consumption calculated.

Meningeal lymphatic ablation.

Visudyne (Bausch Health, NDC code 0187-5600-15) solution used for lymphatic ablation was reconstituted in 7 ml sterile water at 2 mg ml^{-1}, according to the manufacturer's instruction. Mice were anesthetized with ketamine and xylazine solution, administered with 5 µl Visudyne (in its inactive form) via intra-cisterna magna injection and placed on a heating pad to allow the drug to collect in meningeal lymphatic vessels. After 15 min, a midline incision was created in the skin to expose the dorsal side and frontal, parietal and interparietal part of the skull. For ablated groups, Visudyne was then photoconverted locally through intact skull (but opened skin) using a nonthermal 689-nm-wavelength red laser (Coherent Opal Photoactivator, Lumenis) at five points (one at the superior sagittal sinus, one at the confluence of the superior sagittal sinus, two at the transverse sinus, and one at the injection site) with a spot size of <1 mm in diameter, previously demonstrated to be effective[5]. Each point was photoconverted for 83 s to provide a light dose of 50 J/cm^2 at an intensity of 600 mW/cm^2. Sham controls were either injected with the same volume of Visudyne or received sterile aCSF plus laser treatment. For lymphatic vessel off-target photoactivation with Visudyne, the laser was aimed at five spots outside the lymphatic vasculature (spots are highlighted in Extended Data Fig. 1a). The skin was then sutured, postsurgery analgesic (2 mg kg^{-1} ketoprofen, Zoetis, NADA#140-269) and antibiotic (2.5 mg kg^{-1} Baytril, Bayer, 9012) solutions were administered and mice were allowed to recover on heating pads until fully awake. Behavior experiment results in Fig. 1 were replicated using both sham treatments in separate experiments. For microglia sequencing and histology, aCSF was used as a control.

Intra-cisterna magna injections.

Intra-cisterna magna injections were performed on mice secured in a stereotaxic frame, under ketamine (100 mg kg^{-1}) and xylazine (10 mg kg^{-1}, AnaSed, NADA#139-236) anesthesia. The incision area on the back of the neck was shaved, cleaned with iodine antiseptic and ophthalmic ointment applied on the eyes. Upon making an incision in the skin at midline, the muscle layers retracted and the volume of the desired solution was injected into the CSF-filled cisterna magna using a Hamilton syringe with a 33-G needle. After holding the needle in place for 2 min to prevent backflow, it was removed and the neck skin sutured. Mice were administered analgesic (2 mg kg^{-1} ketoprofen) and antibiotic (2.5 mg kg^{-1} Baytril) solutions and allowed to recover on heating pads until fully awake.

Author Manuscript Author Manuscript Author Manuscript Author Manuscript

AAV delivery.

All AAV vectors were purchased from Vector BioLabs (custom production). For brain endothelium conditional KO experiments, AAV-BR1-CAG-Cre or AAV-BR1-CAG-GFP were administered by 5×10^{11} genomic copies per mouse by tail vein injection and allowed 1 week for vector expression[50]. For enhancement of meningeal lymphatic function in aged mice, 10^{13} genomic copies of AAV1-CMV-VEGF-C or AAV1-CMV-LacZ was delivered i.c.m. in 2 μl aCSF as described in Intra-cisterna magna injections above. Following i.c.m. virus injection, mice were allowed at least one month to achieve AAV expression and enhancement of meningeal lymphatic function before behavioral assessment[5].

Microglia and macrophage depletion.

Normal chow was replaced with food containing PLX5622 (plexxikon, D1100404i) for 2 weeks to deplete CSF1-dependent myeloid cells. Experimental controls were placed on identical feed formulation except lacking the drug PLX5622 (ref.[51]). Depletion was verified by immunohistochemistry for Iba1 (Fig. 2 and Immunohistochemistry section).

ELISA.

Following lethal dose of anesthetic, blood was collected from the retroorbital sinus after removing the eye and placed in tubes with 50 ul heparin (1,000 USP U ml^{-1}), pooling two mice per replicate. Cells are removed from plasma by centrifugation for 10 min at 1,000 *g* and 4 °C. ELISA was performed on the supernatant using Invitrogen IL-1 beta Mouse ELISA Kit (BMS611) per the manufacturer's instructions.

Microglia isolation and single-cell sequencing.

Mice were given a lethal dose of anesthetic and perfused with ice-cold PBS with 5 U ml^{-1} heparin. Immediately following perfusion, whole brain was harvested, and meninges were removed as much as possible and divided by hemisphere for dual analysis pipelines. One hemisphere from each brain was immediately drop fixed in 4% paraformaldehyde solution for histological analysis while the other hemisphere was suspended in ice-cold PBS for microglia isolation. At this point, hemispheres from five biological replicates were pooled per condition. Following tissue collection, PBS was decanted, and tissue was dissociated in 5 ml Hank's buffering saline solution (Sigma-Aldrich, H9269) with DNaseI (50 U ml^{-1}, Thermo Fisher Scientific, EN051) and papain (4 U ml^{-1}, Worthington Biochemical, LS003126) at 37 °C for 45 min. Cell suspension was then passed through a 70-μm strainer, and $CD11b^{+}$ cells were magnetically sorted using CD11b MicroBeads, human and mouse (Miltenyi, 130-126-725) as per manufacturer's instructions using AutoMACS (Miltenyi, 130-092-545). Due to increased levels of cellular debris in aged samples, the cell suspension was run over the magnetic sorting column twice. Enriched microglia samples were then submitted to the University of Virginia Genome Analysis and Technology Core for single-cell library preparation and sequencing using the 10x Genomics Chromium platform for gel bead in emulsion and complementary DNA generation with the Chromium Single Cell 3' Library & Gel Bead Kit v2. Libraries were sequenced on the Illumina NextSeq using pair-ended sequencing, targeting a depth of 100,000 reads per cell.

Author Manuscript Author Manuscript Author Manuscript Author Manuscript

Single-cell RNA-sequencing analysis.

Base call files were converted to Cellranger compatible fastq files using the Illumina Bcl2fastq software. Reads were then aligned to the mm10 transcriptome using the Cellranger software pipeline (version 2.2.0) provided by 10x Genomics, specifically the count function with expected counts of 2,000 cells per sample. The resulting filtered gene by cell matrices of unique molecular identifier (UMI) counts for each sample were read into R using the read10xCounts function from the Droplet Utils package and young and old samples were merged separately by gene symbol into two dataframes[52]. Further filtering was applied in order to exclude genes expressed in 5 or fewer cells and remove low quality cells. In the young samples, cells were excluded if they had fewer than 1,000 or greater than 50,000 UMI counts, cells expressing fewer than 500 unique genes, as well as cells with greater than 10% mitochondrial gene expression. In the aged samples, cells were excluded if they had fewer than 500 or greater than 35,000 UMI counts, cells expressing fewer than 500 or greater than 6,000 unique genes, as well as cells with greater than 15% mitochondrial gene expression. Expression values for the remaining cells were then normalized using the scran and scater packages and the resulting $\log_2$ values were transformed to the natural log scale for compatibility with the Seurat (v3.1.1) pipeline. Aged and young samples were then integrated with the use of FindIntegrationAnchors and IntegrateData from the Seurat package. Expression values were scaled across each gene, the effects of sequencing depth per cell and number of unique features were regressed out, and principal components analysis was applied. Based on the statistical significance of the principal components, calculated with the jackstraw test, and the percentage of variance explained by each, the first 10 components were chosen for *t*-stochastic neighbor embedding and shared nearest neighbor clustering. Optimization of the Louvain algorithm applied to the shared nearest neighbor graph as implemented in the FindClusters function with resolution set to 0.2 resulted in 11 clusters, which were annotated manually based on canonical gene markers. For analysis of differentially expressed genes between conditions, each cluster was filtered to include genes that had at least five transcripts in at least five cells, and then the top 2,000 highly variable genes were determined and included for further analysis using the SingleCellExperiment modelGeneVar and getTopHVG functions. After filtering, observational weights for each gene were calculated using the ZINB-WaVE zinbFit and zinbwave functions[53]. These genes were then included in the edgeR model, which was created with the glmFit function, by using the glmWeightedF function[54]. Results were then filtered using Benjamini–Hochberg adjusted *P* value threshold of less than 0.05 as statistically significant. Volcano plots were made with the EnhancedVolcano package[55]. Overrepresentation enrichment analysis with Fisher's exact test was used to determine significantly enriched gene ontology terms (adjusted $P < 0.05$) for the sets of significantly differentially expressed genes between conditions. For each gene set, genes were separated into up- and downregulated and separately[56], the enrichGO function from the clusterProfiler package was used with a gene set size between 10 and 500 genes and *P* values were adjusted using the Benjamini–Hochberg correction[57].

Statistical analysis and reproducibility.

No statistical methods were used to recalculate or predetermine sample sizes. Data distribution was assumed to be normal, but this was not formally tested. Data collection

Author Manuscript Author Manuscript Author Manuscript Author Manuscript

and analysis were performed by an investigator blinded to the identity of the experimental groups. Animals with the same genetic background (for example C57BL6) were randomly divided into two groups during the surgical procedure or injection: a control and a treated group (e.g., sham versus ablation, saline versus IL1-β, or AAV-GFP versus AAV-VEGF-C). The random allocation of conditional KOs mice (e.g., Cre^- and Cre^+ littermates) was driven by Mendelian inheritance. Mice of different experimental groups were housed in mixed cages and never kept in separate cages. Two-group comparisons were made using two-tailed unpaired Student's *t*-test or Mann–Whitney tests. For comparisons of multiple factors (e.g., young versus aged, sham and ablated, saline or IL-1β treated), two-way ANOVA or three-way ANOVA was used followed by a post hoc test as indicated. All statistical tests used for group or cluster comparisons in single-cell RNA-sequencing experiment analysis are specified in Methods. Statistical outliers were identified using ROUT test ($Q = 0.5\%$) and excluded from the analysis. An outlier was identified and excluded in Fig. 1c, in the ablation-IL-1β group; two outliers were identified in Extended Data Fig. 1b in the aCSF-IL-1β group; three outliers were identified in Fig. 3i, two in the control group and one in the VEGF-C group; and one outlier identified in Fig. 3j in the control group at 6 h. Data and graphs are represented as mean ± s.e.m. Statistical analysis and graph plotting was performed using Prism 9.2.0 (GraphPad Software) or R software (version 3.5.0).

Author Manuscript
Author Manuscript
Author Manuscript
Author Manuscript

Extended Data

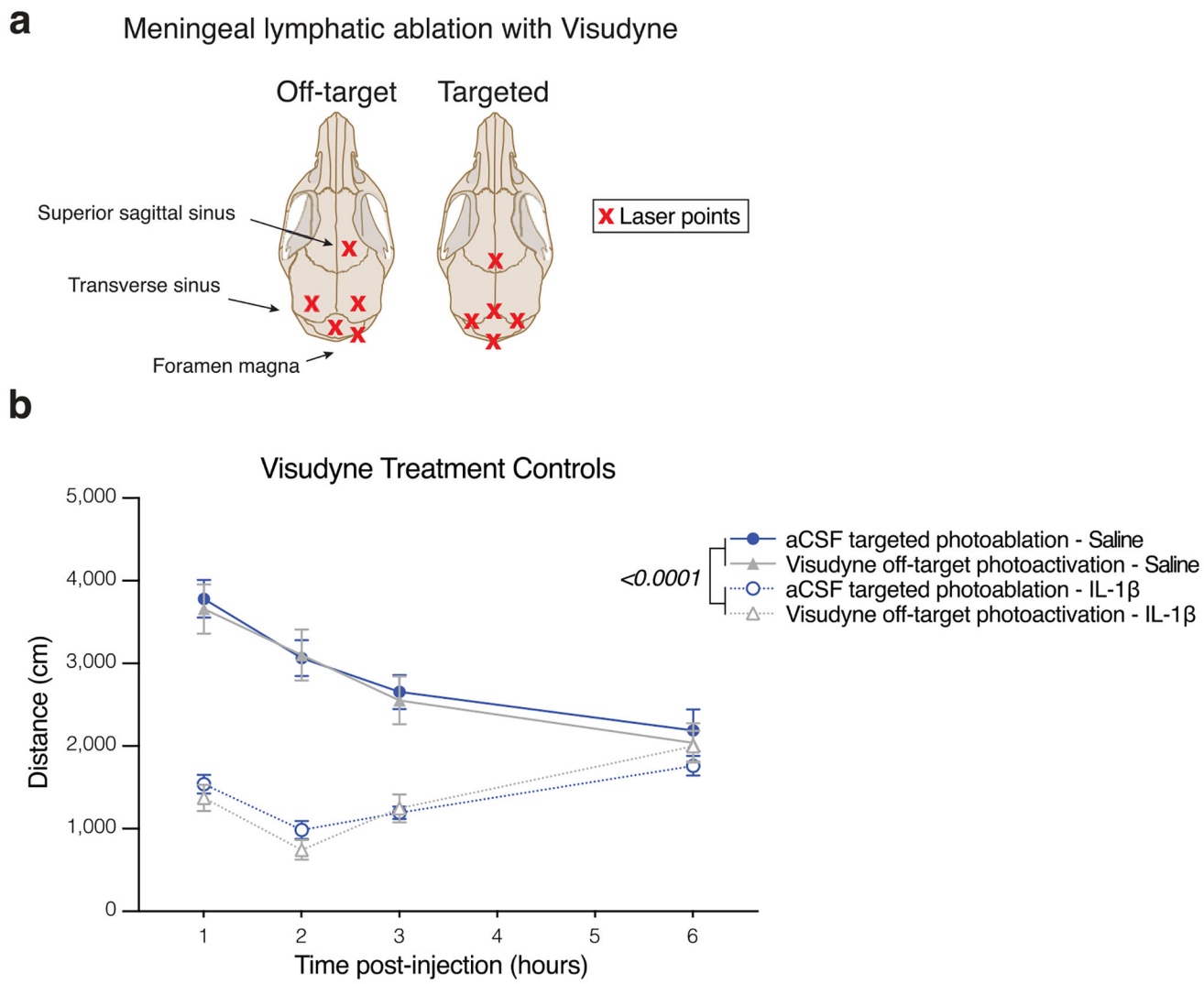

Extended Data Fig. 1 |. Off-target effects of Visudyne do not contribute to behavioral response to peripheral IL-1β.

a, Schematic view of dorsal skull. Crosses mark the location of photoactivation with non-thermal laser. Off-target sites were chosen for their lack of meningeal vasculature. **b**, Locomotor activity one week following artificial cerebrospinal fluid (aCSF) and targeted photoablation, or Visudyne and off-target photoactivation. Mice were injected with 1 ug IL-1β or saline intraperitoneally 1 h before repeated open field assessment (n = 8 mice per group, 2 outliers removed in aCSF – IL-1b by ROUT Q = 0.5%). Data presented as mean ± s.e.m. **b**, Three-way ANOVA. Data in b resulted from a single experiment.

Author Manuscript Author Manuscript Author Manuscript Author Manuscript

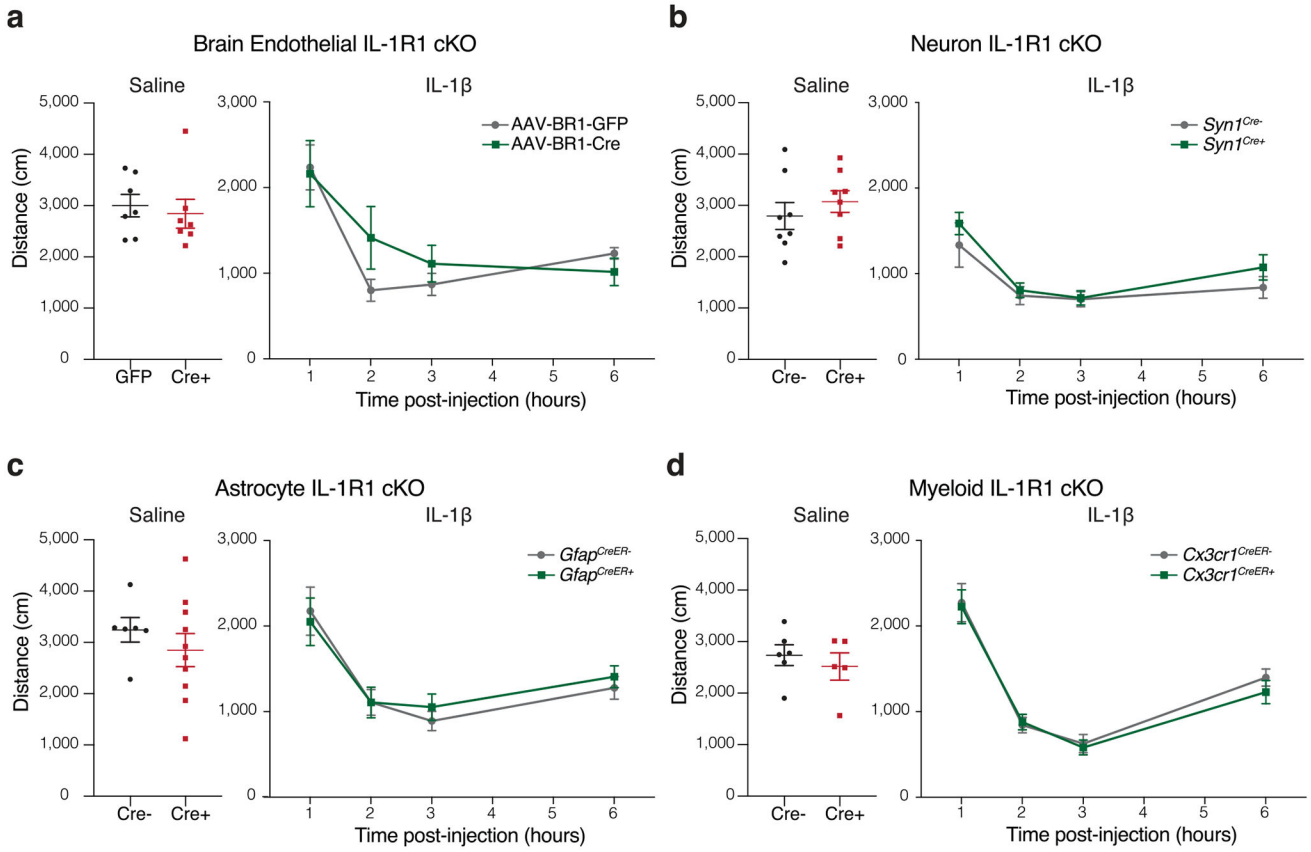

Extended Data Fig. 2 |. IL-1β signaling on endothelial cells, neurons, astrocytes and microglia is not required for behavioral response to peripheral IL-1β.

a–d, Locomotor activity following saline (left) or IL-1β i.p. injection (right) in conditional knockout mice. **a**, Brain endothelium was targeted by injection of AAV-BR1-GFP or AAV1-BR1-Cre into IL-1R$^{fl/fl}$ mice (n = 7 per group), or (**b-d**) by crossing floxed mice to cell specific Cre lines: **b**, neurons (*Syn1*^{Cre}, n = 8 mice per group), **c**, astrocytes (n = 6 *Gfap*$^{CreER-}$ and n = 10 *Gfap*$^{CreER+}$ mice for saline, n = 15 *Gfap*$^{CreER-}$ and n = 13 *Gfap*$^{CreER+}$ mice for IL-1β), and **d**, myeloid (n = 6 *Cx3cr1*$^{CreER-}$ and n = 5 *Cx3cr1*$^{CreER+}$ mice for saline, n = 17 *Cx3cr1*$^{CreER-}$ and n = 11 *Cx3cr1*$^{CreER+}$ for IL-1β). Data presented as mean ± s.e.m.. Two-way ANOVA. The experiments in a–d were repeated in duplicates, and one experimental set of data is presented. No significant difference was found between groups.

Author Manuscript
Author Manuscript
Author Manuscript
Author Manuscript

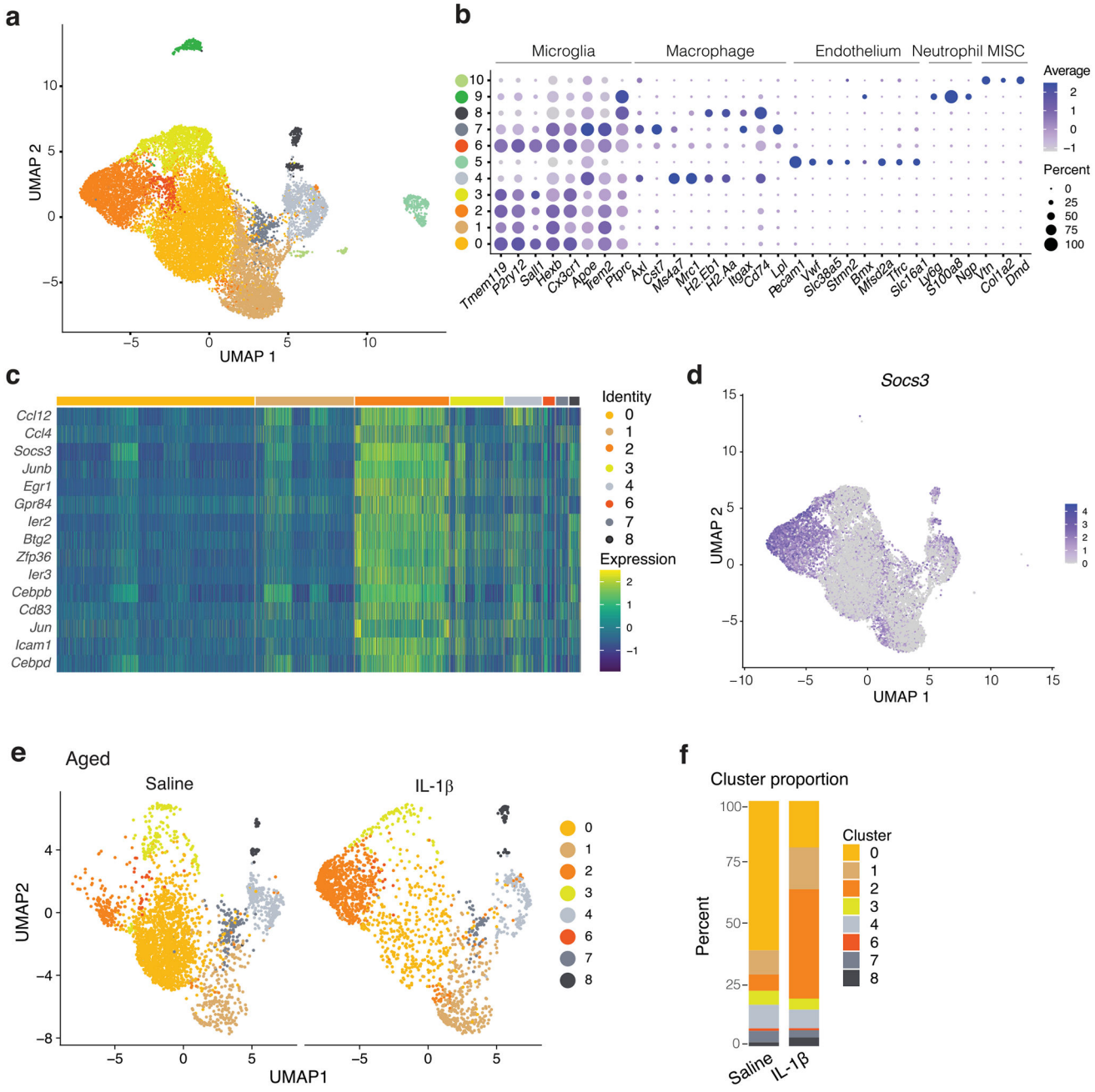

Extended Data Fig. 3 |. Gene expression analysis by single-cell sequencing of microglia after IL-1β induced sickness.

a, UMAP representation for brain CD11b^{+} cells highlighting the different clusters with and without lymphatic ablation and injected with saline or IL-1β. **b**, Dot plot of cell type marker expression by cluster. **c**, Heatmap of mean expression of genes used to define inflammatory microglia. **d**, Features plot depicts the distribution of *Socs3* expression. **e**, UMAP representation of CD11b^{+} sequenced cells from 24-month-old aged mice 2 h following saline or IL-1β i.p. injection. **f**, Cluster distribution compared between saline and IL-1β treatment.

Author Manuscript Author Manuscript Author Manuscript Author Manuscript

Supplementary Material

Refer to Web version on PubMed Central for supplementary material.

Acknowledgements

We thank S. Smith for editing the manuscript and E. Griffin and N. Al-Hamadani for animal care and colony maintenance. We thank all members of the Kipnis laboratory for their valuable comments during numerous discussions of this work and the University of Virginia Genome Analysis and Technology Core for single-cell sequencing and consultation on experimental design. This work was funded by the National Institutes of Health grants DP1AT010416 and R37AG034113 to J.K. The funder had no role in study design, data collection and analysis, decision to publish, or preparation of the manuscript.

Data availability

Single-cell RNA-sequencing data are accessible at the Gene Expression Omnibus under the accession number GSE168756. The data underlying the findings in this study are available as source data published alongside as XLSX files. Genetic material used for this paper are available from the authors upon reasonable request.

References

1. Dantzer R Neuroimmune interactions: from the brain to the immune system and vice versa. Physiol. Rev 98, 477–504 (2018). [PubMed: 29351513]
2. Kirsten K, Soares SM, Koakoski G, Carlos Kreutz L & Barcellos LJG Characterization of sickness behavior in zebrafish. Brain Behav. Immun 73, 596–602 (2018). [PubMed: 29981831]
3. Liu X et al. Cell-type-specific interleukin 1 receptor 1 signaling in the brain regulates distinct neuroimmune activities. Immunity 50, 317–333.e316 (2019). [PubMed: 30683620]
4. Louveau A et al. Structural and functional features of central nervous system lymphatic vessels. Nature 523, 337–341 (2015). [PubMed: 26030524]
5. Da Mesquita S et al. Functional aspects of meningeal lymphatics in ageing and Alzheimer's disease. Nature 560, 185–191 (2018). [PubMed: 30046111]
6. Konsman JP, Kelley K & Dantzer R Temporal and spatial relationships between lipopolysaccharide-induced expression of Fos, interleukin-1beta and inducible nitric oxide synthase in rat brain. Neuroscience 89, 535–548 (1999). [PubMed: 10077334]
7. Bluthé RM, Dantzer R & Kelley KW Interleukin-1 mediates behavioural but not metabolic effects of tumor necrosis factor alpha in mice. Eur. J. Pharmacol 209, 281–283 (1991). [PubMed: 1839150]
8. Cremona S, Goujon E, Kelley KW, Dantzer R & Parnet P Brain type I but not type II IL-1 receptors mediate the effects of IL-1 beta on behavior in mice. Am. J. Physiol 274, R735–R740 (1998). [PubMed: 9530240]
9. Ellul P, Boyer L, Groc L, Leboyer M & Fond G Interleukin-1 β-targeted treatment strategies in inflammatory depression: toward personalized care. Acta Psychiatr. Scand 134, 469–484 (2016). [PubMed: 27744648]
10. Dantzer R Cytokine, sickness behavior, and depression. Neurol Clin 24, 441–460 (2006). [PubMed: 16877117]
11. Lu S et al. Elevated specific peripheral cytokines found in major depressive disorder patients with childhood trauma exposure: a cytokine antibody array analysis. Compr. Psychiatry 54, 953–961 (2013). [PubMed: 23639406]
12. Koo JW & Duman RS Evidence for IL-1 receptor blockade as a therapeutic strategy for the treatment of depression. Curr. Opin. Investig. Drugs 10, 664–671 (2009).
13. Mota R et al. Interleukin-1β is associated with depressive episode in major depression but not in bipolar disorder. J. Psychiatr. Res 47, 2011–2014 (2013). [PubMed: 24074516]

Author Manuscript Author Manuscript Author Manuscript Author Manuscript

14. Walker AK, Wing EE, Banks WA & Dantzer R Leucine competes with kynurenine for blood-to-brain transport and prevents lipopolysaccharide-induced depression-like behavior in mice. Mol. Psychiatry 24, 1523–1532 (2019). [PubMed: 29988087]
15. Ching S et al. Endothelial-specific knockdown of interleukin-1 (IL-1) type 1 receptor differentially alters CNS responses to IL-1 depending on its route of administration. J. Neurosci 27, 10476–10486 (2007). [PubMed: 17898219]
16. Bluthé RM, Michaud B, Kelley KW & Dantzer R Vagotomy blocks behavioural effects of interleukin-1 injected via the intraperitoneal route but not via other systemic routes. Neuroreport 7, 2823–2827 (1996). [PubMed: 8981475]
17. Godbout JP et al. Aging exacerbates depressive-like behavior in mice in response to activation of the peripheral innate immune system. Neuropsychopharmacology 33, 2341–2351 (2008). [PubMed: 18075491]
18. Godbout JP et al. Exaggerated neuroinflammation and sickness behavior in aged mice following activation of the peripheral innate immune system. FASEB J 19, 1329–1331 (2005). [PubMed: 15919760]
19. Abraham J & Johnson RW Central inhibition of interleukin-1beta ameliorates sickness behavior in aged mice. Brain Behav. Immun 23, 396–401 (2009). [PubMed: 19152833]
20. Holmes C et al. Systemic infection, interleukin 1beta, and cognitive decline in Alzheimer's disease. J. Neurol. Neurosurg. Psychiatry 74, 788–789 (2003). [PubMed: 12754353]
21. Wilson JE et al. Delirium. Nat Rev Dis Primers 6, 90 (2020). [PubMed: 33184265]
22. Lampe IK, Kahn RS & Heeren TJ Apathy, anhedonia, and psychomotor retardation in elderly psychiatric patients and healthy elderly individuals. J Geriatr Psychiatry Neurol 14, 11–16 (2001). [PubMed: 11281310]
23. JW. L & V. B Tables of Summary Health Statistics for the U.S. Population: 2018 National Health Interview Survey National Center for Health Statistics, (Centers for Disease Control and Prevention, 2019).
24. Pavon JM et al. Accelerometer-measured hospital physical activity and hospital-acquired disability in older adults. J. Am. Geriatr. Soc 68, 261–265 (2020). [PubMed: 31747050]
25. Louveau A et al. CNS lymphatic drainage and neuroinflammation are regulated by meningeal lymphatic vasculature. Nat. Neurosci 21, 1380–1391 (2018). [PubMed: 30224810]
26. Rustenhoven J et al. Functional characterization of the dural sinuses as a neuroimmune interface. Cell 184, 1000–1016.e1027 (2021). [PubMed: 33508229]
27. Ding XB et al. Impaired meningeal lymphatic drainage in patients with idiopathic Parkinson's disease.Nat. Med 27, 411–418 (2021). [PubMed: 33462448]
28. Arnone D et al. Role of Kynurenine pathway and its metabolites in mood disorders: A systematic review and meta-analysis of clinical studies. Neurosci. Biobehav. Rev 92, 477–485 (2018). [PubMed: 29940237]
29. Banks WA, Ortiz L, Plotkin SR & Kastin AJ Human interleukin (IL) 1 alpha, murine IL-1 alpha and murine IL-1 beta are transported from blood to brain in the mouse by a shared saturable mechanism. J. Pharmacol. Exp. Ther 259, 988–996 (1991). [PubMed: 1762091]
30. Dantzer R Cytokine, sickness behavior, and depression. Immunol. Allergy Clin. North Am 29, 247–264 (2009). [PubMed: 19389580]
31. Zhu L et al. Interleukin-1 causes CNS inflammatory cytokine expression via endothelia-microglia bi-cellular signaling. Brain Behav. Immun 81, 292–304 (2019). [PubMed: 31228609]
32. Zeisel A et al. Molecular architecture of the mouse nervous system. Cell 174, 999–1014 (2018). [PubMed: 30096314]
33. Kettenmann H, Hanisch UK, Noda M & Verkhratsky A Physiology of microglia. Physiol. Rev 91, 461–553 (2011). [PubMed: 21527731]
34. Marsh SE et al. Dissection of artifactual and confounding glial signatures by single-cell sequencing of mouse and human brain. Nat. Neurosci 25, 306–316 (2022). [PubMed: 35260865]
35. Elmore MR et al. Colony-stimulating factor 1 receptor signaling is necessary for microglia viability, unmasking a microglia progenitor cell in the adult brain. Neuron 82, 380–397 (2014). [PubMed: 24742461]

Author Manuscript Author Manuscript Author Manuscript Author Manuscript

36. Lei F et al. CSF1R inhibition by a small-molecule inhibitor is not microglia specific; affecting hematopoiesis and the function of macrophages. Proc. Natl Acad. Sci. U S A 117, 23336–23338 (2020). [PubMed: 32900927]
37. Kokona D, Ebneter A, Escher P & Zinkernagel MS Colony-stimulating factor 1 receptor inhibition prevents disruption of the blood-retina barrier during chronic inflammation. J. Neuroinflammation 15, 340 (2018). [PubMed: 30541565]
38. Vichaya EG et al. Microglia depletion fails to abrogate inflammation-induced sickness in mice and rats. J. Neuroinflammation 17, 172 (2020). [PubMed: 32475344]
39. Da Mesquita S et al. Meningeal lymphatics affect microglia responses and anti-Aβ immunotherapy. Nature 593, 255–260 (2021). [PubMed: 33911285]
40. Song E et al. VEGF-C-driven lymphatic drainage enables immunosurveillance of brain tumours. Nature 577, 689–694 (2020). [PubMed: 31942068]
41. Bonsall DR et al. Suppression of locomotor activity in female C57Bl / 6J mice treated with interleukin-1\beta: investigating a method for the study of fatigue in laboratory animals. PLoS One 10, e0140678 (2015). [PubMed: 26469939]
42. Merali Z, Brennan K, Brau P & Anisman H Dissociating anorexia and anhedonia elicited by interleukin-1beta: antidepressant and gender effects on responding for “free chow” and “earned” sucrose intake. Psychopharmacology (Berl.) 165, 413–418 (2003). [PubMed: 12459927]
43. Johnston M, Wakeling A, Graham N & Stokes F Cognitive impairment, emotional disorder and length of stay of elderly patients in a district general hospital. Br J Med Psychol 60, 133–139 (1987). [PubMed: 3620390]
44. Abdi S, Spann A, Borilovic J, de Witte L & Hawley M Understanding the care and support needs of older people: a scoping review and categorisation using the WHO international classification of functioning, disability and health framework (ICF). BMC Geriatr 19, 195 (2019). [PubMed: 31331279]
45. Herrera-Pérez JJ, Martínez-Mota L & Fernández-Guasti A Aging increases the susceptibility to develop anhedonia in male rats. Prog. Neuropsychopharmacol. Biol. Psychiatry 32, 1798–1803 (2008). [PubMed: 18722496]
46. Onaolapo OJ et al. Exogenous testosterone, aging, and changes in behavioral response of gonadally intact male mice. J. Exp. Neurosci 10, 59–70 (2016). [PubMed: 27158222]
47. Bonsall DR et al. Suppression of locomotor activity in female C57Bl/6J mice treated with interleukin-1β: investigating a method for the study of fatigue in laboratory animals. PLoS One 10, e0140678 (2015). [PubMed: 26469939]
48. Malatynska E et al. Anhedonic-like traits and lack of affective deficits in 18-month-old C57BL/6 mice: implications for modeling elderly depression. Exp. Gerontol 47, 552–564 (2012). [PubMed: 22583982]
49. Liu MY et al. Sucrose preference test for measurement of stress-induced anhedonia in mice. Nat. Protoc 13, 1686–1698 (2018). [PubMed: 29988104]
50. Körbelin J et al. A brain microvasculature endothelial cell-specific viral vector with the potential to treat neurovascular and neurological diseases. *EMBO* Mol. Med 8, 609–625 (2016).
51. Cronk JC et al. Peripherally derived macrophages can engraft the brain independent of irradiation and maintain an identity distinct from microglia. J. Exp. Med 215, 1627–1647 (2018). [PubMed: 29643186]
52. Lun ATL et al. EmptyDrops: distinguishing cells from empty droplets in droplet-based single-cell RNA sequencing data. Genome Biol 20, 63 (2019). [PubMed: 30902100]
53. Van den Berge K et al. Observation weights unlock bulk RNA-seq tools for zero inflation and single-cell applications. Genome Biol 19, 24 (2018). [PubMed: 29478411]
54. Robinson MD, McCarthy DJ & Smyth GK edgeR: a Bioconductor package for differential expression analysis of digital gene expression data. Bioinformatics 26, 139–140 (2010). [PubMed: 19910308]
55. Blighe K, Rana S & Lewis M EnhancedVolcano: Publication-Ready Volcano Plots with Enhanced Colouring and Labeling R package version 1.14.0; https://github.com/kevinblighe/EnhancedVolcano (2020).

Author Manuscript Author Manuscript Author Manuscript Author Manuscript

56. Hong G, Zhang W, Li H, Shen X & Guo Z Separate enrichment analysis of pathways for up- and downregulated genes. J. R. Soc. Interface 11, 20130950 (2014).

57. Yu G, Wang LG, Han Y & He QY clusterProfiler: an R package for comparing biological themes among gene clusters. OMICS 16, 284–287 (2012). [PubMed: 22455463]

Author Manuscript Author Manuscript Author Manuscript Author Manuscript

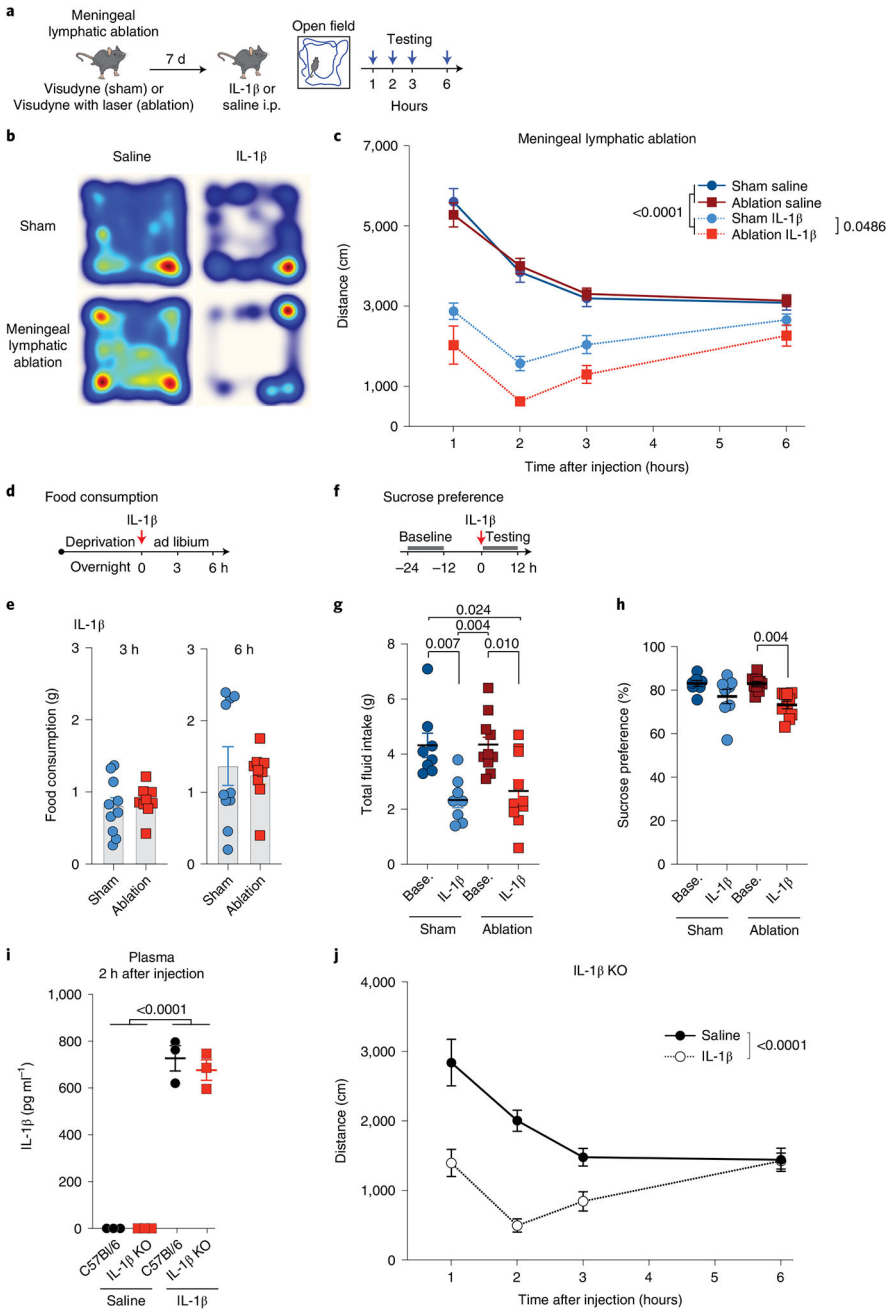

Fig. 1 |. Meningeal lymphatic ablation exacerbates sickness behavior.

a, Experimental scheme involving 2-month-old male mice injected with Visudyne intra-cisterna magna (i.c.m.) and photoactivated for ablation or without photoactivation for sham. Seven days later, IL-1β-induced sickness behavior was quantified by repeated 10-min open field test at 1, 2, 3 and 6 h following 1 μg IL-1β or saline i.p. injection. **b**, Representative heatmaps depict mouse position over 10 min, 2 h following saline or IL-1β injection. **c**, Exploratory activity of lymphatic ablated and sham mice following saline or IL-1β injection (n = 8 sham with saline, n = 7 ablation with saline, n = 8 sham with IL-1β, n = 6 ablation with IL-1β-injected male mice). **d**,**e**, Food consumption of mice with different treatments, 3

Author Manuscript Author Manuscript Author Manuscript Author Manuscript

and 6 h after IL-1β i.p. injection (n = 10 sham, n = 9 ablation). **f**–**h**, Sucrose preference as compared with baseline and IL-1β-treated groups for sham and ablation measured for 12 h (n = 8 sham, n = 10 ablation-treated mice). Base., baseline. **g**, No difference in total fluid intake was seen between sham and ablation groups in either the baseline or IL-1β-treated groups. **h**, Sucrose preference as compared with baseline for each group. **i**, IL-1β detected by enzyme-linked immunosorbent assay (ELISA) of plasma from IL-1β KO and WT mice 2 h following IL-1β or saline i.p. injection (n = 3 samples consisting of plasma from two pooled male mice each). **j**, Exploratory activity of IL-1β KO mice following IL-1β or saline injection (n = 8 male mice per group). **c**, Three-way analysis of variance (ANOVA). **e**, Two-tailed unpaired Mann–Whitney test. **g, h**, Two-way ANOVA with Tukey's post hoc test. **i**, Two-way ANOVA with Tukey's post hoc test. **j**, Two-way ANOVA with Sidak's post hoc test. Data in panels **c, e, g, i**, and **j** are presented as mean ± s.e.m. The experiments in panels **c**, **i** and **j** were repeated in duplicates, and one experimental set of data is presented. Data in panels **e**, **g** and **h** resulted from a single experiment.

Author Manuscript Author Manuscript Author Manuscript Author Manuscript

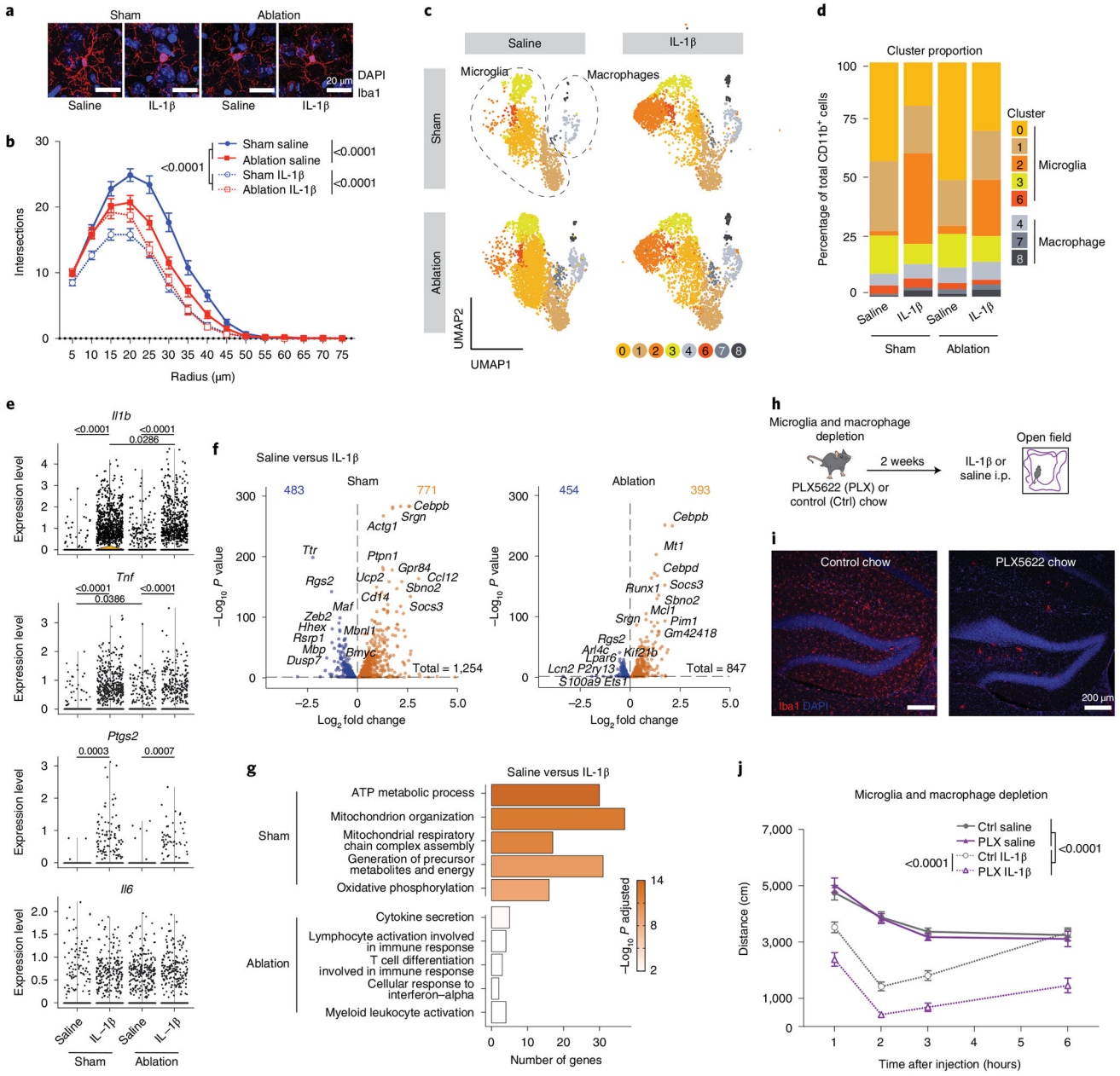

Fig. 2 |. Meningeal lymphatic ablation worsens sickness behavior through microglia.

a, Representative confocal images of brain sections stained for Iba1 (red) and 4,6-diamidino-2-phenylindole (DAPI, blue) 2 h following IL-1β or saline injection comparing photoactivation of Visudyne (ablation) or aCSF (sham) injected 3-month-old mice. Scale bars, 20 μm. **b**, Sholl analysis of microglia complexity for each condition (n = 45 cells from three mice per group). **c**–**g**, Transcriptomes of enriched CD11b$^+$ brain cells from ablation (Visudyne with photoactivation)- and sham (aCSF with photoactivation)-treated mice, 2 h after IL-1β or saline injection, as analyzed by single-cell RNA sequencing (n = 5 mice per group). **c**, Uniform manifold approximation and projection (UMAP) illustrating microglia and macrophages split by experimental conditions (clusters 5, 9 and 10 were removed and

Author Manuscript Author Manuscript Author Manuscript Author Manuscript

are identified in Extended Data Fig. 3). **d**, Representation of microglia and macrophage cluster proportions for each condition (n = 5 mice per group). **e**, Violin plots showing normalized transcript counts of the expression of *Il1b*, *Tnf*, *Ptgs2* and *Il6* in microglia (clusters 0, 1, 2, 3 and 6 combined). **f**, Volcano plots depicting significantly downregulated (blue) and upregulated (orange) genes between saline and IL-1β treatments for sham- and ablation-treated mice. **g**, Top five upregulated gene ontology terms enriched in sham (out of 302 total) and ablation (out of 42 total) in response to IL-1β by lowest adjusted P value. **h**–**j**, Experimental scheme for microglia and macrophage depletion strategy using PLX5622 (PLX) chow for 2 weeks. **i**, Representative confocal images of brain sections stained for Iba1 and DAPI. Scale bars, 200 μm. **j**, Exploratory activity of microglia- and macrophage-depleted and control mice following IL-1β or saline i.p. injection (n = 8 male mice per group). Data in panels **b** and **j** presented as mean ± s.e.m. **b, j**, Three-way AVOVA. **d**, Two-proportion Z-test to compare the percentage in cluster 2. **e**,**f**, Differently expressed genes were identified using a two-tailed F-test with adjusted degrees of freedom based on weights calculated per gene with a zero-inflation model. **g**, One-tailed Fisher's exact test. **d**–**g**, P value adjustment with Benjamini–Hochberg. **b**, **h**–**j**, the experiments were repeated in duplicates, and one experimental set of data is presented. Data in panels **c**–**g** resulted from a single experiment.

Author Manuscript Author Manuscript Author Manuscript Author Manuscript

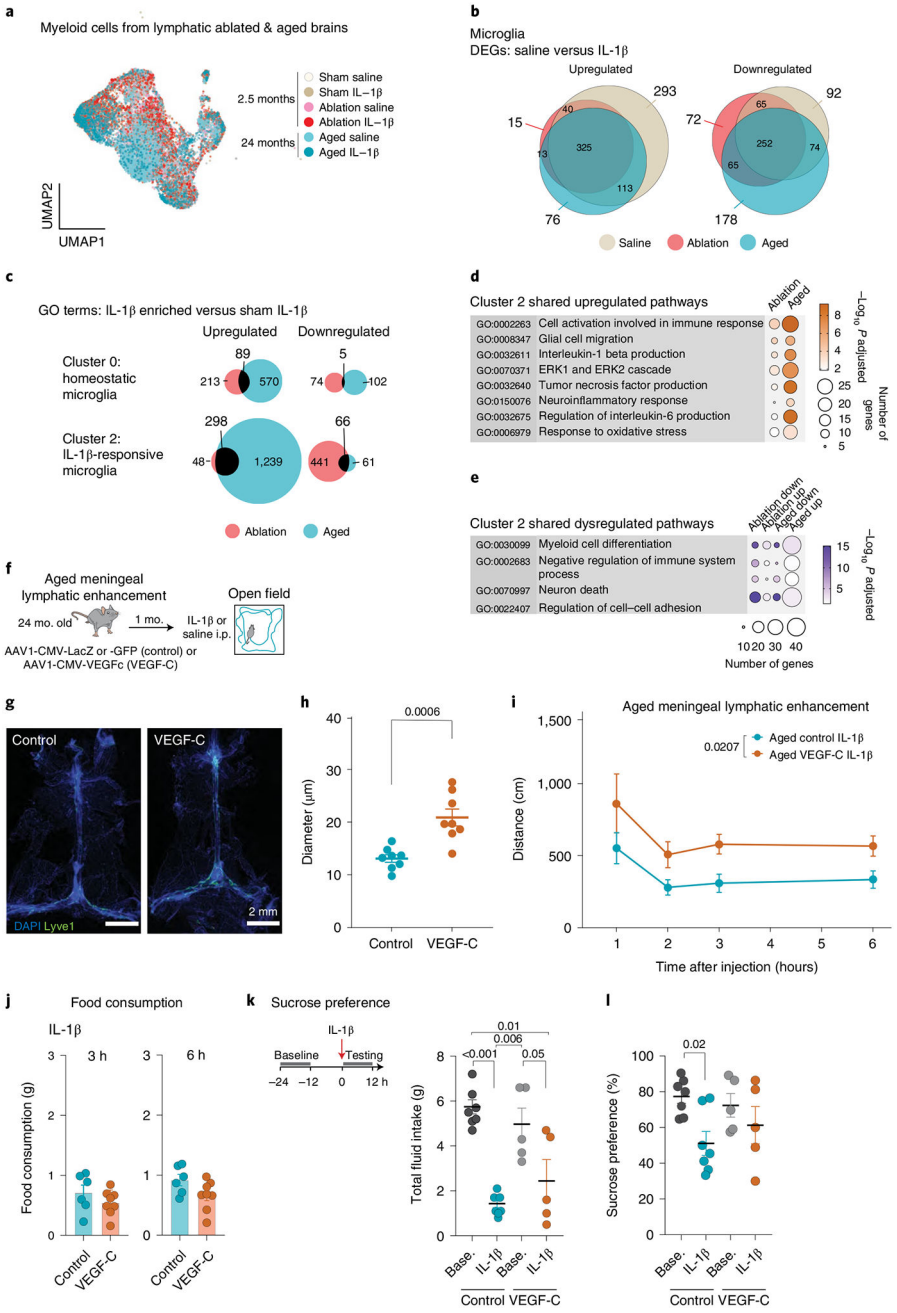

Fig. 3 |. Enhancement of meningeal lymphatic function in aged mice improves exploratory behavior during sickness.

a–**e**, Data from 24-month-old mice were integrated into the data set shown in Fig. 2b–g. **a**, UMAP depicting the distribution of cells across conditions. **b**, Overlap in upregulated and downregulated differentially expressed genes (DEGs) between microglia in saline and IL-1β treatments. **c**, Gene ontology (GO) terms in IL-1β-enriched (ablation versus IL-1β, aged versus IL-1β) compared with adult control (sham versus IL-1β). Quantification of the overlap in upregulated and downregulated pathways is shown for cluster 0 (homeostatic microglia) and cluster 2 (IL-1β-associated microglia). **d**, Significantly elevated pathways in

Author Manuscript Author Manuscript Author Manuscript Author Manuscript

meningeal lymphatic ablation and aged cluster 2 microglia over adult control. **e**, Four out of 25 dysregulated pathways in cluster 2 that are both elevated and reduced in lymphatic ablation and aging compared to sham. **f–l**, AAV1-CMV-LacZ, AAV1-CMV-GFP (sham) or AAV1-CMV-VEGF-C was administered to aged mice by i.c.m. injection to achieve meningeal enhancement of lymphatic function after 1 month and IL-1β injected i.p. **g**, Representative confocal images of dural brain meninges stained for Lyve-1 and DAPI. Scale bars, 2 mm. **h**, Quantification of the meningeal lymphatic vessel diameter after VEGF-C treatment ($n = 8$ mice per group). **i**, Exploratory activity of aged lymphatic-enhanced (VEGF-C) and control mice following IL-1β i.p. injection ($n = 8$ mice per group). **j**, Food consumption, 3 and 6 h after IL-1β i.p. injection ($n = 6$ control, $n = 8$ VEGF-C-treated mice). **k**, Total intake of water and sucrose for 12 h before and after IL-1β injection ($n = 7$ control, $n = 5$ VEGF-C-treated mice). **l**, Sucrose preference of IL-1β injected mice as compared with baseline for control and VEGFC-treated groups of mice shown in panel **k**. Data in panels **h–l** are represented as mean ± s.e.m. **b**, DEGs were identified using a two-tailed *F*-test with adjusted degrees of freedom based on weights calculated per gene with a zero-inflation model. **c–e**, One-tailed Fisher's exact test. **b–e**, *P* value adjustment with Benjamini–Hochberg. **h**, Two-tailed unpaired Student's *t*-test. **i**, Two-way ANOVA. Data in panels **a–e** and **j–l** resulted from a single experiment. Experiments in panels h and i were repeated in duplicates, and one experimental set of data is presented.